ACS APPLIED MATERIALS & INTERFACES

www.acsami.org Research Article

Controlling Magnon Interaction by a Nanoscale Switch

Arezoo Etesamirad, Rodolfo Rodriguez, Joshua Bocanegra, Roman Verba, Jordan Katine, Ilya N. Krivorotov, Vasyl Tyberkevych, Boris Ivanov, and Igor Barsukov*

Cite This: *ACS Appl. Mater. Interfaces* 2021, 13, 20288–20295

Read Online

ACCESS | Metrics & More | Article Recommendations

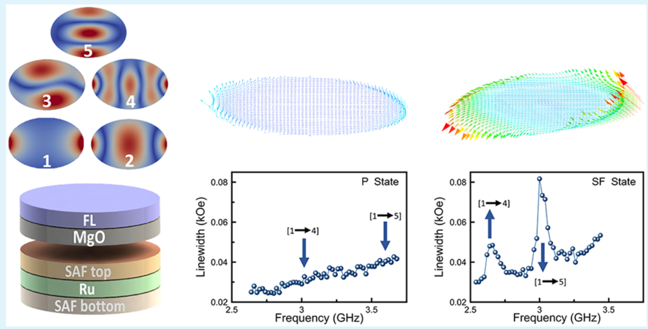

ABSTRACT: The ability to control and tune magnetic dissipation is a key concept of emergent spintronic technologies. Magnon scattering processes constitute a major dissipation channel in nanomagnets, redefine their response to spin torque, and hold the promise for manipulating magnetic states on the quantum level. Controlling these processes in nanomagnets, while being imperative for spintronic applications, has remained difficult to achieve. Here, we propose an approach for controlling magnon scattering by a switch that generates nonuniform magnetic field at nanoscale. We provide an experimental demonstration in magnetic tunnel junction nanodevices, consisting of a free layer and a synthetic antiferromagnet. By triggering the spin-flop transition in the synthetic antiferromagnet and utilizing its stray field, magnon interaction in the free layer is toggled. The results open up avenues for tuning nonlinearities in magnetic neuromorphic applications and for engineering coherent magnon coupling in hybrid quantum information technologies.

KEYWORDS: *spin wave, magnon interaction, spin torque, magnetic tunnel junction, stray field, magnetic neuromorphic systems, hybrid quantum systems*

INTRODUCTION

Many spintronic technologies are based on the idea of manipulating the magnetization of a nanoscale magnet by spin torque. Spin torque drives magnetic reversal in nonvolatile spin-torque memory[1−5] and auto-oscillations in spin-torque oscillators while competing with magnetic dissipation.[6−9] Magnon scattering processes play a major role in this context. They lead to redistribution[10,11] of energy among magnon modes and determine magnetization dynamics at large excitation levels[12−14] which are of particular importance for spintronics applications.[15−17] In nanomagnets—the building blocks of the latter—the discrete magnon spectrum leads to unusual phenomena that are qualitatively different from those in bulk and thin films.[18−20] In particular, three-magnon scattering has been recently shown[21] to invert the response of a nanomagnet to spin torque, thus impinging on the main working principle of many spintronics technologies.

Magnon scattering is also responsible for parametric pumping,[22] soliton formation, phase locking, and other instrumental phenomena of magnetization dynamics.[15,16,23] Controlling magnon scattering processes[24] would allow for tuning the nonlinear response of nanomagnets employed in neuromorphic magnetic systems.[25−27] Moreover, it would provide a path for engineering coherent magnon coupling[28−30] in hybrid quantum information applications.[31] Functionalization of nanomagnets critically depends on our ability to control magnon interaction at the nanoscale, which has remained difficult to achieve.[32,33]

Here, we demonstrate that magnon scattering in a nanomagnet can be efficiently controlled by an adjacent synthetic antiferromagnet that acts as a nanoscale switch. By triggering spin-flop transition in the synthetic antiferromagnet and by utilizing its nonuniform stray field, we achieve to toggle the degenerate three-magnon scattering in the nanomagnet.

In nanoscale ferromagnets, standing spin waves form due to geometrical confinement; the magnon spectrum at gigahertz frequencies is discrete. In this study, we consider a thin ferromagnetic nanodisk with elliptical cross section as a model nanomagnet. Its spin wave modes correspond to the normal modes[34] of a disk (Figure 1A). We number the modes in ascending order of their frequency, starting with $|n = 1\rangle$ for the lowest frequency f_1 mode which has excitation maxima at the tips of the ellipse. With increasing mode number n, one and more excitation nodes appear within the disk plane. The

Received: January 24, 2021
Accepted: April 8, 2021
Published: April 22, 2021

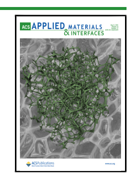

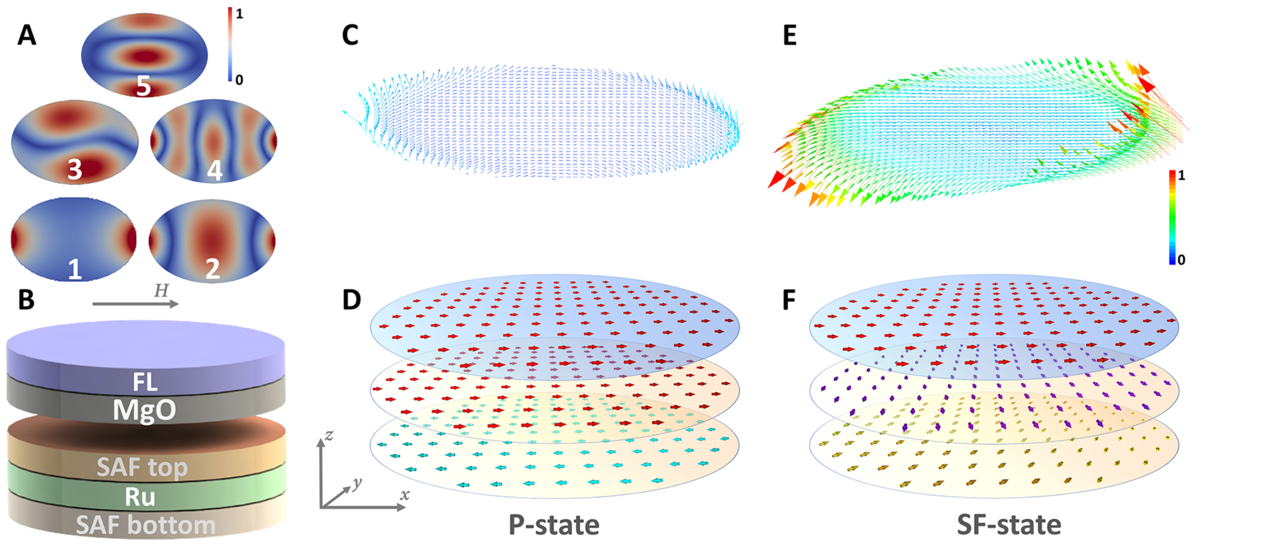

Figure 1. (A) Lateral profiles of the spin wave modes in the free layer (FL), obtained from micromagnetic simulations of the magnetic tunnel junction (100×150 nm^2 MTJ) nanodevice, sketched in (B). (C) Stray field from the SAF at the position of the FL in the parallel state. (D) Static magnetization in the parallel state. (E) SAF's stray field in the spin-flop state with the corresponding static magnetization in (F). Magnetic field H is applied along the major axis of the elliptical device (x-axis).

frequency of the modes depends on magnetic field. When the frequency ratio of two modes is nearly f_i:f_j = 1:2, two magnons of the lower frequency mode $|i\rangle$ can confluence into one magnon of the higher frequency mode $|j\rangle$. This constitutes a degenerate three-magnon (3M) process which, due to its technological relevance,[17,21,32] we shall focus on in what follows.

Besides the energy conservation requirement given by the frequency ratio, the 3M scattering is determined by the strength of interaction between the magnon modes involved in the process.[21,32,35] In nanomagnets possessing the symmetry of an orthogonal coordinate system (e.g., rectangular, circular, and elliptical)[36] and with negligible magnetic anisotropy, the number of 3M processes allowed by symmetry is greatly reduced, as recently shown in refs 32, 35, and 37. However, irregularities of demagnetization field at the nanomagnet's edges, as well as inevitable structural imperfections,[1,38] can diminish the symmetry restrictions and lead to a finite, albeit small, magnon interaction. Application of a local nonuniform magnetic field to the nanomagnet has a similar symmetry-breaking effect, but it can result in a drastic increase of the magnon interaction, be done in a controlled manner, and used as a tool to engineer magnon scattering. The applied field must exhibit nonuniformity at the length scales of the nanomagnet and therefore itself originate from a nanoscale source.

■ RESULTS AND DISCUSSION

To validate the proposed concept, we employ a magnetic tunnel junction nanopillar of elliptical layers with 150 nm × 100 nm cross section and ∼1−2 nm thickness, sketched in Figure 1B and detailed in the Methods section. The device consists of a ferromagnetic free layer (FL), an MgO tunneling layer, and a synthetic antiferromagnet (SAF). The latter is composed of two ferromagnetic layers coupled by antiferromagnetic RKKY interaction[39,40] through a Ru buffer layer. The bottom layer is exchange-biased along the major axis of the ellipse by an antiferromagnet. All ferromagnetic layers consist of CoFeB compounds, endued with easy-plane magnetic anisotropy.[41] Because of the shape anisotropy, the major axis of the ellipse is the magnetic easy-axis.

With magnetic field applied in the easy-axis, we measure the resistance of the device, which is governed by the tunneling magnetoresistance across the MgO layer.[8,42,43] As shown in Figure 2, the resistance presents with a nearly rectangular

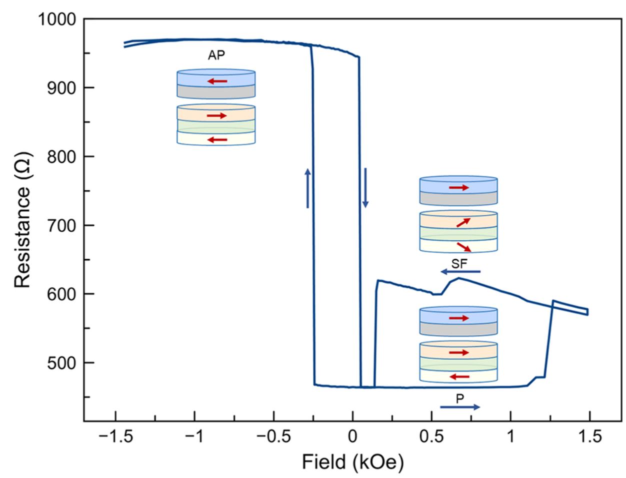

Figure 2. MTJ nanodevice resistance, as a function of field applied in the easy-axis, shows switching events between antiparallel (AP), parallel (P), and spin-flop (SF) state.

hysteresis loop near zero field. At negative fields, the device is in the high-resistance, antiparallel (AP)-state. By increasing the field to 0.04 kOe, the free layer switches by 180° and the device arrives in the low-resistance, parallel (P)-state (Figure 1D). With further increasing the field to 1.21 kOe, the SAF undergoes spin-flop transition[44] (Figure 1F) and the device enters into the intermediate-resistance, spin-flop (SF)-state. After reversing the direction of the field sweep, the device lingers in the SF-state until 0.16 kOe. Then the SAF layers align opposite to each other; this corresponds to the P-state of the device (Figure 1D). By further sweeping the field

https://doi.org/10.1021/acsami.1c01562
ACS Appl. Mater. Interfaces 2021, 13, 20288−20295

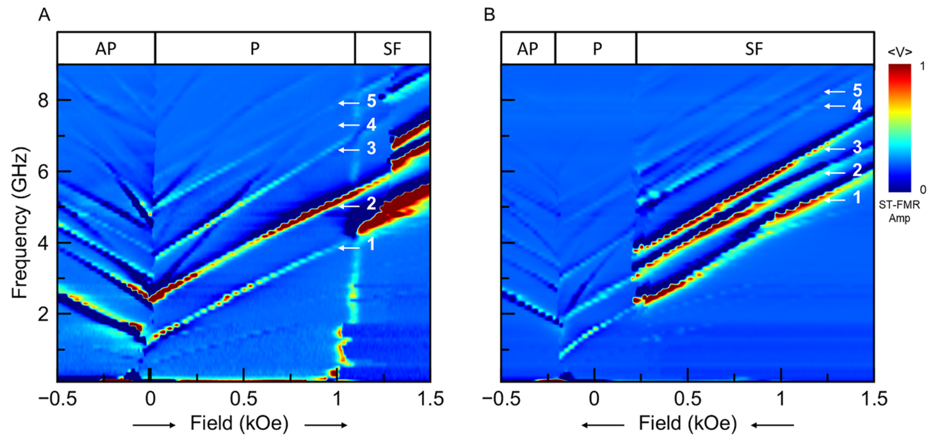

Figure 3. Spin-torque ferromagnetic resonance measurements carried out by sweeping the field from negative to positive values (A) and from positive to negative values (B). The magnon modes present with the same frequency−field slope (faint lines with doubled slope correspond to parasitic second-harmonic signals). The field regions of the parallel (P), antiparallel (AP), and spin-flop (SF) states are indicated; magnon modes are numbered. All measurements are performed at room temperature.

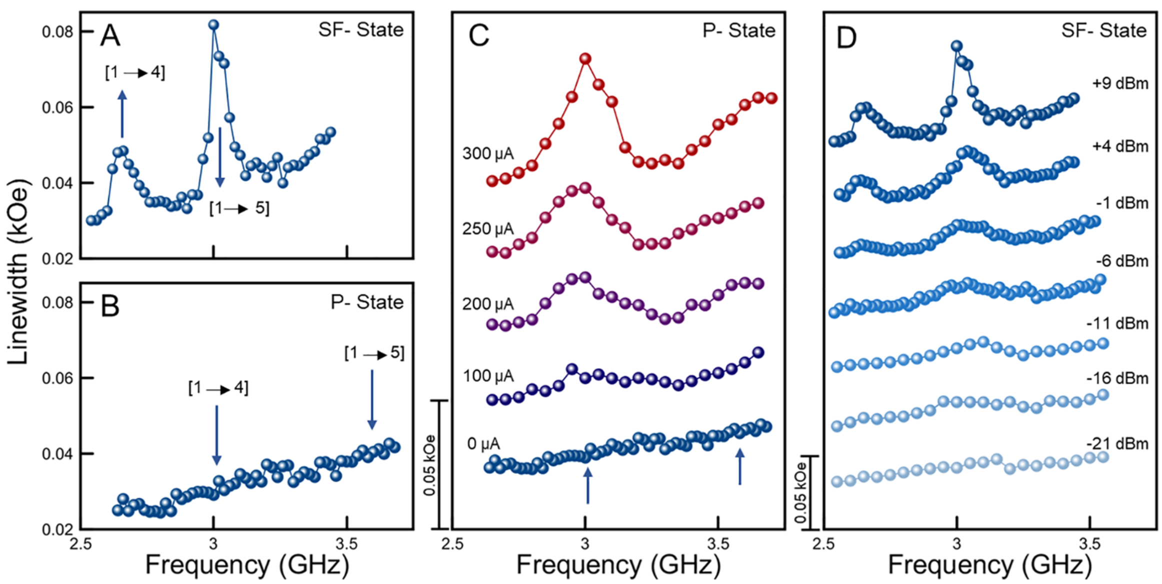

Figure 4. (A) In the spin-flop state, the line width of mode |1⟩ exhibits two peaks due to the three-magnon processes. The labels $[i \to j]$ indicate positions for which the frequency ratio of the participating modes f_i:f_j = 1:2 is found. (B) In the parallel state, the three-magnon scattering rates are negligibly small; no peaks in the line width are observed. (C) However, with increasing dc bias current and the associated antidamping spin torque, the three-magnon scattering rates in the parallel state are enhanced. (D) In the spin-flop state, at zero dc bias, the line width peaks fade away with decreasing microwave power.

backward, the free layer undergoes reversal of the zero-field loop, and the device arrives in the AP-state.

In the P-state (Figure 1D), the stray field from the SAF at the position of the free layer (Figure 1C) is small—the fields from the top and bottom layer of the SAF in MTJs are engineered to largely cancel each other.[1,3,45] Upon the spin-flop transition, however, the SAF's stray field increases and presents with a pronounced nonuniformity at nanoscale (compare Figures 1C and 1E). We utilize the hysteretic behavior of the SAF to controllably switch this field. While we use external magnetic field to drive the spin-flop transition in this work, various nanoscale switches driven by other external stimuli such as spin current, electric field, strain, and temperature are generally possible.

To investigate the magnon spectra, we use field-modulated spin-torque ferromagnetic resonance (ST-FMR).[43] The measurements are first performed by sweeping the field from negative to positive values; the data are shown in Figure 3A. Several excitations with nearly linear frequency−field relation are observed. Because the FL and SAF layers possess very different effective magnetic anisotropy energies (due to RKKY interaction and exchange bias; see the Methods section), their magnon modes are well separated in energy. As detailed in refs 43 and 44 the modes shown in Figure 3 correspond to standing spin wave modes which are localized in the free layer and have normal-mode[34] excitation profiles (Figure 1A). At the positive field of 1.21 kOe, the device switches into the spin-flop state. The stray field from the SAF slightly affects the frequencies and the separation of the magnon modes. This effect suggests a small yet noticeable modification of the FL micromagnetic state and/or its magnon modes.

We repeat the ST-FMR measurements—now sweeping the field from positive to negative values. The magnon spectrum shown in Figure 3B is similar to the forward sweep in Figure

https://doi.org/10.1021/acsami.1c01562
ACS Appl. Mater. Interfaces 2021, 13, 20288−20295

3A. However, the switching from spin-flop state to parallel state takes place at ∼0.2 kOe. The SF-state occupies a larger field range. In what follows, we investigate magnon processes within the hysteretic field region of 0.2−1.2 kOe, where the device can be controllably brought in two distinct regimes of the P-state and SF-state.

The line width of a magnon mode represents its dissipation rate. We evaluate the line width of the main mode $|1\rangle$, shown in Figure 4. In the spin-flop state, the line width presents with a peak at the characteristic field 0.35 kOe (2.65 GHz), for which we find the frequency ratio f_1:f_4 = 1:2 for the modes $|1\rangle$ and $|4\rangle$. Here, two magnons of the mode $|1\rangle$ confluence into one magnon of the mode $|4\rangle$, constituting a degenerate three-magnon process that we label as $[1 \rightarrow 4]$. At another characteristic field of 0.5 kOe (3 GHz), a peak that corresponds to the $[1 \rightarrow 5]$ process is observed. These peaks represent an increased dissipation rate due to the 3M process that is resonant in the frequency detuning $2f_i - f_j$ of the participating modes, as derived in ref 21. The frequency detuning becomes zero and the dissipation peaks at the characteristic 3M fields.

Now, we evaluate the line width in the parallel state, as shown in Figure 4B. The frequency ratios f_1:f_4 = 1:2 and f_1:f_5 = 1:2 are maintained at slightly shifted fields 0.6 kOe (3 GHz) and 0.8 kOe (3.6 GHz) and allow for the same $[1 \rightarrow 4]$ and $[1 \rightarrow 5]$ processes. However, the line width does not exhibit peaks at the characteristic fields. Because the 3M process is a nonlinear phenomenon that becomes more prominent at larger excitations, we increase the microwave power. However, even at high excitation levels leading to device destruction, the 3M peaks of the line width cannot be realized.

To make sure that the $[1 \rightarrow 4]$ and $[1 \rightarrow 5]$ processes are present in the P-state but just small in magnitude (scattering rate), we subject the device to dc bias current that results in a nominal antidamping spin torque. The antidamping spin torque leads to line width reduction (115 MHz/mA) at field values far away from the characteristic three-magnon fields, where the 3M process is virtually inactive. In the 3M regime near the characteristic fields, on the other hand, the effect of the antidamping spin torques is inverted. With increasing antidamping spin torque, the effective susceptibility of both modes, $|i\rangle$ and $|j\rangle$, increases. As detailed in ref 21, the modes begin to participate in the 3M process at a higher rate. While the intrinsic dissipation continues to be reduced by the antidamping spin torque, the nonlinear effect of the 3M process dominates and increases the total dissipation. As shown in Figure 4C, at the characteristic 3M fields, we in fact find that the effective dissipation increases in response to the antidamping spin torque and presents with two peaks. This inversion of the spin-torque effect is inherent to the resonant 3M process[21] and confirms that they are indeed present in both the parallel and spin-flop state. In the P-state, however, the 3M scattering rate is negligibly small (unless enhanced by spin torque).

This result validates the proposed concept of controlling magnon interaction via symmetry-breaking local magnetic field. To assess magnon interaction, the normalized vector field of the static magnetization $\vec{\mu}(\vec{r})$ and dynamic magnetization of individual magnon modes $\vec{s}(\vec{r})$ must be considered. The magnetic Hamiltonian term, which describes the confluence of two $|i\rangle$ magnons into one $|j\rangle$ magnon (as well as the inverse process), is $\mathcal{H}^{(3)} = \psi_{ij} a_i a_i a_j^* + \psi_{ij}^* a_i^* a_i^* a_j$, with a being the mode amplitude.[21] Using the vector Hamiltonian approach,[35,46] we can write the magnon interaction coefficient ψ_{ij} as

$$\psi_{ij} \sim \int 2(\vec{s}_i \cdot \vec{s}_j^*)\vec{\mu} \cdot \hat{N} \cdot \vec{s}_i + (\vec{s}_i \cdot \vec{s}_i)\vec{\mu} \cdot \hat{N} \cdot \vec{s}_j^* \, \mathrm{d}^3 r \tag{1}$$

The interaction is largely related to dipolar coupling between the magnons, and the operator $\hat{N}$ can be written in the integral form

$$\hat{N} = \int \hat{G}(\vec{r}, \vec{r}') \, \mathrm{d}^3 r' \tag{2}$$

with the magnetostatic Green's function kernel having components $\hat{G}_{\alpha\beta'}(\vec{r}, \vec{r}') = -\frac{1}{4\pi}\partial_\alpha \partial_{\beta'} |\vec{r} - \vec{r}'|^{-1}$. The diagonal components of the integral kernel are symmetric in space, while off-diagonal ones are antisymmetric. With the FL magnetized along the x-axis, only N_{xy} contributes to the 3M scattering. As a consequence of the spatial antisymmetry of this component, 3M confluence from mode $|1\rangle$ into laterally totally antisymmetric modes should have a sizable scattering rate, while confluence into symmetric modes is prohibited.[32,35,37] Because the modes $|4\rangle$ and $|5\rangle$ are almost but not perfectly symmetric, their small scattering rate in the parallel state is consistent with the theoretical picture.

In general, application of the SAF's stray field in the SF-state has a manifold effect on the 3M scattering. First, the static magnetization can tilt away from the easy-axis (high-symmetry) direction, which allows the diagonal components (N_{xx} and N_{yy}) to contribute to the magnon interaction and to lift the symmetry restrictions for the magnon modes. This effect can be further amplified by the reduced symmetry of the static magnetization vector field. In particular, while maintaining the central symmetry $\vec{\mu}(\vec{r}) = \vec{\mu}(-\vec{r})$, it can lose axial symmetry, e.g., $\vec{\mu}(x,y) = \vec{\mu}(-x,y)$. Second, the SAF's stray field with nonuniformity at nanoscale can directly break magnon modes' symmetry and blend their symmetric or antisymmetric character.[47,48]

Our micromagnetic simulations[49] show a very small change to the FL static magnetization vector field upon application of the SAF's stray field. The tilt of the magnetization is negligible, and the variation of the vector field at the edges of the FL disk is small ($\langle 1 - \mu_x \rangle_\mathrm{P} = 13 \times 10^{-4}$ and $\langle 1 - \mu_x \rangle_\mathrm{SF} = 18 \times 10^{-4}$ in Figure 1F). Modification of the mode separation in Figure 3, however, indicates that this small change of the micromagnetic state and the presence of the nonuniform stray field from the SAF are sufficient to affect the mode structure. The micromagnetic simulations on the rather complex multilayer structure of the MTJ device do not allow for a reliable quantitative consideration of the mode structure for the calculation of mode interaction ψ. Yet, we can assess the resulting effect experimentally.

Generally, the 3M scattering rate depends[21] on the product $g{\cdot}\psi$ of magnon excitation level g and interaction ψ between the magnon modes that participate in the 3M process. We carry out microwave power dependent measurements at zero dc bias current. With decreasing power p in the spin-flop state (Figure 4D), the line width peak fades away. It takes over 30 dB of power reduction for the line width peak to subside and for the 3M scattering rate to reach the value of the parallel state. We estimate an enhancement of the $g{\cdot}\psi$ product between parallel and spin-flop state of $(g_\mathrm{SF}{\cdot}\psi_\mathrm{SF})$:$(g_\mathrm{P}{\cdot}\psi_\mathrm{P}) > 35$.

The spin waves in the MTJ nanodevice are excited by microwave Oersted fields and high-frequency spin torques.[50,51]

https://doi.org/10.1021/acsami.1c01562
ACS Appl. Mater. Interfaces 2021, 13, 20288−20295

The excitation level g is thus not just a function of the microwave power, $g \propto \sqrt{p}$, but also increases with the effective angle ϕ between magnetic moments of the free layer and the SAF top layer.[52] To account for that, we assess the amplitude of the ST-FMR signal in the parallel and spin-flop state. The measurements are performed as a function of the microwave power at field values outside of the three-magnon regime and result in the ratio of ST-FMR amplitudes in the spin flop and parallel state of A_{SF}:$A_P \approx 35$.

The amplitude of the ST-FMR signal is generally a function of the magnon excitation level g and the sensitivity of the voltage signal to magnetization oscillations. The latter is composed of photovoltage and photoresistance. In the calibration measurements, no dc current is used; thus, there is no contribution from the photoresistance. The photovoltage is a function of the angle ϕ between the free layer and the top SAF layer. The ST-FMR amplitude can be therefore written as $A \propto g \sin \phi$.

For the spin-flop state, the angle can be extracted from the magnetoresistance measurements (Figure 2) as $\phi_{SF} = 64°$. In the parallel state, the angle ϕ_P can strictly speaking not be treated as zero. The angle assumes a small but finite effective value due to nonuniformity of the magnetization and small misalignment of the magnetic field with respect to the easy-axis. On the basis of micromagnetic simulations and the precision of the sample alignment, we find this angle to be below 1°. However, on the basis of our estimations across multiple samples, for the following calculation, we use the most generous upper limit of $\phi_P < 4°$. By means of this calibration, we find the excitation level in the spin-flop state to be only slightly larger than in the parallel state:

$$\frac{g_{SF}}{g_P} = \frac{A_{SF}}{A_P}\frac{\sin \phi_P}{\sin \phi_{SF}} < 2.7 \tag{3}$$

This conservative estimation reveals the ratio of the mode interaction in the spin-flop and parallel state to be at least ψ_{SF}:$\psi_P > 13$. Such a large difference in magnon coupling leads to the qualitatively different behavior observed in Figure 4A,B. Even at moderately large excitation levels, the modified magnon coupling results in a 200% increase of the effective damping, marking distinct dissipation states of the SF an P states (Figure 4A,B,D).

CONCLUSIONS

In conclusion, we achieve a controlled toggling of the magnon interaction by at least 1 order of magnitude. By means of a magnetic field that is nonuniform at the nanoscale, the symmetry restrictions for magnon scattering processes are diminished and the scattering rate is modified. While further theoretical and experimental studies are called upon to elucidate the quantitative connection between the magnon scattering, the micromagnetic state of the nanomagnet, and the symmetry of the stray field, this work demonstrates engineering of magnon interaction in a magnet of nanoscale size. We generate the local field by exploiting hysteretic spin-flop transition of a synthetic antiferromagnet. Other nanodevices based on spin-torque, thermal, and voltage-driven switching are envisioned. The distinct dissipative states that result from modified magnon interaction add functionality to spin-torque applications such as spin-torque memory,[1−5] spin-torque oscillators,[6−9] microwave detectors,[17] and spin-wave-based logic.[53] In the emerging paradigm of magnetic neuromorphic networks,[25−27] the nonlinear response of magnetic neurons plays a central role. Magnon scattering processes[32] offer a route to achieving such nonlinearity, which can be tuned by controlled magnon interaction as developed in this work. Furthermore, magnon processes have the potential to provide nonlinear capabilities to spin-based hybrid quantum systems, for which efficient control of magnon interaction is a prerequisite and allows for engineering coherent magnon coupling.

METHODS

MTJ Devices and Micromagnetic Simulations. The devices were fabricated on thermally oxidized Si wafers. By use of magnetron sputtering, the following layer stack was deposited: (15)PtMn antiferromagnetic layer, (2.3)$Co_{70}Fe_{30}$ SAF bottom layer, (0.85)Ru RKKY-layer, (2.4)$Co_{40}Fe_{40}B_{20}$ SAF top layer, (1)MgO tunneling layer, and (1.8)$Co_{20}Fe_{60}B_{20}$ free layer. The numbers in parentheses indicate the thickness of the layers in nanometers. The layer stack was seeded and capped by (5)Ta layers and electric leads. The devices were defined by using electron-beam lithography and etched by using ion milling to an elliptical pillars (with lateral dimensions of 150 nm × 100 nm for the device shown here). The devices were subject to thermal annealing at 300 °C for 2 h in a magnetic field applied along the major axis of the ellipse. The annealing procedure defined the exchange bias field of the SAF bottom layer to point along the $-x$ direction.

Micromagnetic simulations were performed by using MuMax code.[49] The magnetization of the layers was set to values obtained from magnetometry performed on film-level control samples: FL = 1630 emu/cm^3, SAF top = 1400 emu/cm^3, and SAF bottom = 1900 emu/cm^3. The volume exchange interaction was set to 13 pJ/m, the RKKY exchange interaction between the SAF top and SAF bottom layers was set to −5 fJ/m. The SAF bottom layer is exchange-biased by the PtMn antiferromagnet, which was modeled via a unidirectional anisotropy field of −0.045T along the x-axis, and by a uniaxial anisotropy of 60×10^3 J/m^3.

Because of the different magnetization values, as well as additional contributions of RKKY interaction and exchange bias to the effective magnetic anisotropy, the magnetic anisotropy energies of the FL and the SAF layers are very different. The magnon modes of the free layer and the SAF layers are thus well separated in energy. The observed effects were confirmed not to originate from magnon−magnon interaction of the free layer and the SAF layers. The three-magnon model was validated experimentally on multiple MTJ devices with positive and negative perpendicular anisotropies and various magnetic configurations of the SAF.[21,43]

Because of the incommensurability of the nominal thicknesses and the simulation cell size of 1 nm × 1 nm × 1 nm, the magnetization in the simulation was scaled by the ratio of the nominal and simulated thickness. This discrepancy leads to implicit inaccuracy of the effective shape anisotropy and the interplay of the Zeeman effect and the RKKY interaction. The simulated switching fields, shown in Figure 5, can therefore not exactly match the experimental values. The RKKY interaction value and the unidirectional anisotropy field (exchange bias) at the SAF bottom layer were manually adjusted until the simulated switching behavior qualitatively resembled the experimental data in Figure 2. Considering the inaccuracies due to meshing and a simplified magnetic anisotropy model, the behavior is reproduced remarkably well. The static magnetization direction was then implemented into ANSYS finite-element simulation to calculate the stray field of the SAF at the position of the FL, shown in Figure 1. Again, while we cannot reliably calculate the absolute value of the stray field, its relative magnitude in the P- and SF-state and the nonuniformity can be assessed.

After simulating the switching behavior, a sinc-timed pulse of magnetic field was applied to the device. To excite spin wave modes of various spatial symmetries, the pulse was polarized in the out-of-plane direction, had a lateral Gauss shape with ∼20 nm width, and

https://doi.org/10.1021/acsami.1c01562
ACS Appl. Mater. Interfaces 2021, 13, 20288−20295

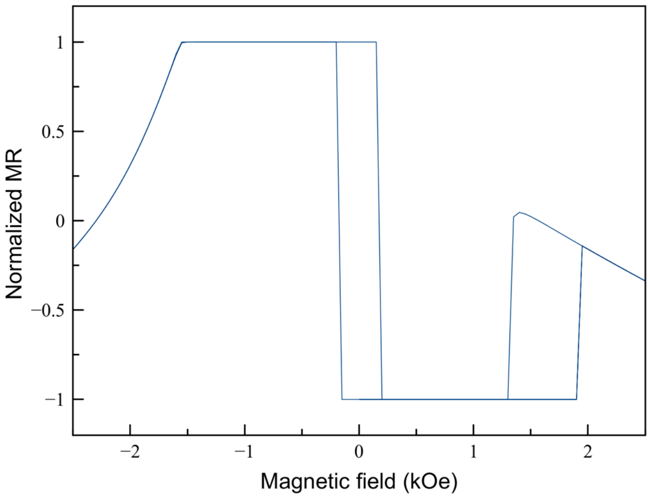

Figure 5. Micromagnetic simulation of the normalized magnetoresistance of the MTJ device. The hysteretic spin flop at positive fields is qualitatively reproduced.

was centered asymmetrically in one of the ellipse quadrants. The decay of magnetization was Fourier-transformed to cell-specific frequency-domain amplitudes which are shown in Figure 1. By evaluating the phase of the Fourier transform, we find that the mode $|1\rangle$ has phase-symmetric excitation maxima. All higher-order modes present with a 180° phase jump across each excitation node.

AUTHOR INFORMATION

Corresponding Author

Igor Barsukov − *Physics and Astronomy, University of California, Riverside, Riverside, California 92521, United States;* orcid.org/0000-0003-4835-5620; Phone: +1-951-827-5343; Email: igorb@ucr.edu

Authors

Arezoo Etesamirad − *Physics and Astronomy, University of California, Riverside, Riverside, California 92521, United States*

Rodolfo Rodriguez − *Physics and Astronomy, University of California, Riverside, Riverside, California 92521, United States*

Joshua Bocanegra − *Physics and Astronomy, University of California, Riverside, Riverside, California 92521, United States*

Roman Verba − *Institute of Magnetism, Kyiv 03142, Ukraine*

Jordan Katine − *Western Digital, San Jose, California 95119, United States*

Ilya N. Krivorotov − *Physics and Astronomy, University of California, Irvine, Irvine, California 92697, United States;* orcid.org/0000-0002-1658-2565

Vasyl Tyberkevych − *Department of Physics, Oakland University, Rochester, Michigan 48309, United States;* orcid.org/0000-0002-8374-2565

Boris Ivanov − *Institute of Magnetism, Kyiv 03142, Ukraine*

Complete contact information is available at: https://pubs.acs.org/10.1021/acsami.1c01562

Notes

The authors declare no competing financial interest.

ACKNOWLEDGMENTS

This work was supported by the National Science Foundation through Grant ECCS-1810541. We thank NVIDIA Corporation for donating a GPU used in this research. R.V. and B.A.I. acknowledge support by National Research Foundation of Ukraine (Grant 2020.02/0261). I.N.K. acknowledges support by the National Science Foundation through Grants DMR-1610146, EFMA-1641989, and ECCS-1708885 and by the Army Research Office through Grant W911NF-16-1-0472.

REFERENCES

(1) Katine, J. A.; Fullerton, E. E. Device Implications of Spin-Transfer Torques. *J. Magn. Magn. Mater.* **2008**, *320*, 1217−1226.

(2) Bedau, D.; Liu, H.; Bouzaglou, J.-J.; Kent, A. D.; Sun, J. Z.; Katine, J. A.; Fullerton, E. E.; Mangin, S. Ultrafast Spin-Transfer Switching in Spin Valve Nanopillars with Perpendicular Anisotropy. *Appl. Phys. Lett.* **2010**, *96*, 022514.

(3) Ikeda, S.; Hayakawa, J.; Lee, Y. M.; Matsukura, F.; Ohno, Y.; Hanyu, T.; Ohno, H. Magnetic Tunnel Junctions for Spintronic Memories and Beyond. *IEEE Trans. Electron Devices* **2007**, *54*, 991−1002.

(4) Yuasa, S.; Fukushima, A.; Yakushiji, K.; Nozaki, T.; Konoto, M.; Maehara, H.; Kubota, H.; Taniguchi, T.; Arai, H.; Imamura, H.; Ando, K.; Shiota, Y.; Bonell, F.; Suzuki, Y.; Shimomura, N.; Kitagawa, E.; Ito, J.; Fujita, S.; Abe, K.; Nomura, K.; Noguchi, H.; Yoda, H. *Future Prospects of MRAM Technologies* **2013**, 3.1.1−3.1.4.

(5) Worledge, D. C.; Hu, G.; Abraham, D. W.; Sun, J. Z.; Trouilloud, P. L.; Nowak, J.; Brown, S.; Gaidis, M. C.; O'Sullivan, E. J.; Robertazzi, R. P. Spin Torque Switching of Perpendicular Ta/CoFeB/MgO-Based Magnetic Tunnel Junctions. *Appl. Phys. Lett.* **2011**, *98*, 022501.

(6) Demidov, V. E.; Urazhdin, S.; Ulrichs, H.; Tiberkevich, V.; Slavin, A.; Baither, D.; Schmitz, G.; Demokritov, S. O. Magnetic Nano-Oscillator Driven by Pure Spin Current. *Nat. Mater.* **2012**, *11*, 1028−1031.

(7) Kiselev, S. I.; Sankey, J. C.; Krivorotov, I. N.; Emley, N. C.; Schoelkopf, R. J.; Buhrman, R. A.; Ralph, D. C. Microwave Oscillations of a Nanomagnet Driven by a Spin-Polarized Current. *Nature* **2003**, *425*, 380.

(8) Deac, A. M.; Fukushima, A.; Kubota, H.; Maehara, H.; Suzuki, Y.; Yuasa, S.; Nagamine, Y.; Tsunekawa, K.; Djayaprawira, D. D.; Watanabe, N. Bias-Driven High-Power Microwave Emission from MgO-Based Tunnel Magnetoresistance Devices. *Nat. Phys.* **2008**, *4*, 803−809.

(9) Evelt, M.; Safranski, C.; Aldosary, M.; Demidov, V. E.; Barsukov, I.; Nosov, A. P.; Rinkevich, A. B.; Sobotkiewich, K.; Li, X.; Shi, J.; Krivorotov, I. N.; Demokritov, S. O. Spin Hall-Induced Auto-Oscillations in Ultrathin YIG Grown on Pt. *Sci. Rep.* **2018**, *8*, 1269.

(10) Hula, T.; Schultheiss, K.; Buzdakov, A.; Körber, L.; Bejarano, M.; Flacke, L.; Liensberger, L.; Weiler, M.; Shaw, J. M.; Nembach, H. T.; Fassbender, J.; Schultheiss, H. Nonlinear Losses in Magnon Transport Due to Four-Magnon Scattering. *Appl. Phys. Lett.* **2020**, *117*, 042404.

(11) Schultheiss, H.; Vogt, K.; Hillebrands, B. Direct Observation of Nonlinear Four-Magnon Scattering in Spin-Wave Microconduits. *Phys. Rev. B: Condens. Matter Mater. Phys.* **2012**, *86*, 054414.

(12) Melkov, G. A.; Slobodianiuk, D. V.; Tiberkevich, V. S.; de Loubens, G.; Klein, O.; Slavin, A. N. Nonlinear Ferromagnetic Resonance in Nanostructures Having Discrete Spectrum of Spin-Wave Modes. *IEEE Magn. Lett.* **2013**, *4*, 4000504.

(13) Guo, F.; Belova, L. M.; McMichael, R. D. Nonlinear Ferromagnetic Resonance Shift in Submicron Permalloy Ellipses. *Phys. Rev. B: Condens. Matter Mater. Phys.* **2015**, *91*, 064426.

(14) Schultheiss, K.; Verba, R.; Wehrmann, F.; Wagner, K.; Körber, L.; Hula, T.; Hache, T.; Kákay, A.; Awad, A. A.; Tiberkevich, V.; Slavin, A. N.; Fassbender, J.; Schultheiss, H. Excitation of Whispering

Gallery Magnons in a Magnetic Vortex. *Phys. Rev. Lett.* **2019**, *122*, 097202.
(15) Slavin, A.; Tiberkevich, V. Nonlinear Auto-Oscillator Theory of Microwave Generation by Spin-Polarized Current. *IEEE Trans. Magn.* **2009**, *45*, 1875−1918.
(16) Muduli, P. K.; Pogoryelov, Y.; Zhou, Y.; Mancoff, F.; Åkerman, J. Spin Torque Oscillators and RF Currents-Modulation, Locking, and Ringing. *Integr. Ferroelectr.* **2011**, *125*, 147−154.
(17) Saino, T.; Kanai, S.; Shinozaki, M.; Jinnai, B.; Sato, H.; Fukami, S.; Ohno, H. Write-Error Rate of Nanoscale Magnetic Tunnel Junctions in the Precessional Regime. *Appl. Phys. Lett.* **2019**, *115*, 142406.
(18) Kobljanskyj, Y.; Melkov, G.; Guslienko, K.; Novosad, V.; Bader, S. D.; Kostylev, M.; Slavin, A. Nano-Structured Magnetic Metamaterial with Enhanced Nonlinear Properties. *Sci. Rep.* **2012**, *2*, 478.
(19) Slobodianiuk, D. V.; Melkov, G. A.; Schultheiss, K.; Schultheiss, H.; Verba, R. V. Nonlinear Ferromagnetic Resonance in the Presence of Three-Magnon Scattering in Magnetic Nanostructures. *IEEE Magn. Lett.* **2019**, *10*, 1−5.
(20) Navabi, A.; Liu, Y.; Upadhyaya, P.; Murata, K.; Ebrahimi, F.; Yu, G.; Ma, B.; Rao, Y.; Yazdani, M.; Montazeri, M.; Pan, L.; Krivorotov, I. N.; Barsukov, I.; Yang, Q.; Amiri, P.; Tserkovnyak, Y.; Wang, K. Control of Spin-Wave Damping in YIG Using Spin Currents From Topological Insulators. *Phys. Rev. Appl.* **2019**, *11*, 034046.
(21) Barsukov, I.; Lee, H. K.; Jara, A. A.; Chen, Y.-J.; Gonçalves, A. M.; Sha, C.; Katine, J. A.; Arias, R. E.; Ivanov, B. A.; Krivorotov, I. N. Giant Nonlinear Damping in Nanoscale Ferromagnets. *Sci. Adv.* **2019**, *5*, eaav6943.
(22) Noack, T. B.; Vasyuchka, V. I.; Bozhko, D. A.; Heinz, B.; Frey, P.; Slobodianiuk, D. V.; Prokopenko, O. V.; Melkov, G. A.; Kopietz, P.; Hillebrands, B.; Serga, A. A. Enhancement of the Spin Pumping Effect by Magnon Confluence Process in YIG/Pt Bilayers. *Phys. Status Solidi B* **2019**, *256*, 1900121.
(23) Gurevich, A. G.; Melkov, G. A. *Magnetization Oscillations and Waves*; CRC Press: 1996.
(24) Divinskiy, B.; Urazhdin, S.; Demokritov, S. O.; Demidov, V. E. Controlled Nonlinear Magnetic Damping in Spin-Hall Nano-Devices. *Nat. Commun.* **2019**, *10*, 5211.
(25) Torrejon, J.; Riou, M.; Araujo, F. A.; Tsunegi, S.; Khalsa, G.; Querlioz, D.; Bortolotti, P.; Cros, V.; Yakushiji, K.; Fukushima, A.; Kubota, H.; Yuasa, S.; Stiles, M. D.; Grollier, J. Neuromorphic Computing with Nanoscale Spintronic Oscillators. *Nature* **2017**, *547*, 428−431.
(26) Tanaka, G.; Yamane, T.; Héroux, J. B.; Nakane, R.; Kanazawa, N.; Takeda, S.; Numata, H.; Nakano, D.; Hirose, A. Recent Advances in Physical Reservoir Computing: A Review. *Neural Netw.* **2019**, *115*, 100−123.
(27) Marković, D.; Leroux, N.; Riou, M.; Abreu Araujo, F.; Torrejon, J.; Querlioz, D.; Fukushima, A.; Yuasa, S.; Trastoy, J.; Bortolotti, P.; Grollier, J. Reservoir Computing with the Frequency, Phase, and Amplitude of Spin-Torque Nano-Oscillators. *Appl. Phys. Lett.* **2019**, *114*, 012409.
(28) Tabuchi, Y.; Ishino, S.; Noguchi, A.; Ishikawa, T.; Yamazaki, R.; Usami, K.; Nakamura, Y. Coherent Coupling Between a Ferromagnetic Magnon and a Superconducting Qubit. *Science* **2015**, *349*, 405−408.
(29) Lachance-Quirion, D.; Wolski, S. P.; Tabuchi, Y.; Kono, S.; Usami, K.; Nakamura, Y. Entanglement-Based Single-Shot Detection of a Single Magnon with a Superconducting Qubit. *Science* **2020**, *367*, 425−428.
(30) Hou, J. T.; Liu, L. Strong Coupling Between Microwave Photons and Nanomagnet Magnons. *Phys. Rev. Lett.* **2019**, *123*, 107702.
(31) Li, Y.; Zhang, W.; Tyberkevych, V.; Kwok, W.-K.; Hoffmann, A.; Novosad, V. Hybrid Magnonics: Physics, Circuits, and Applications for Coherent Information Processing. *J. Appl. Phys.* **2020**, *128*, 130902.
(32) Körber, L.; Schultheiss, K.; Hula, T.; Verba, R.; Fassbender, J.; Kákay, A.; Schultheiss, H. Nonlocal Stimulation of Three-Magnon Splitting in a Magnetic Vortex. *Phys. Rev. Lett.* **2020**, *125*, 207203.
(33) Han, J.; Zhang, P.; Hou, J. T.; Siddiqui, S. A.; Liu, L. Mutual Control of Coherent Spin Waves and Magnetic Domain Walls in a Magnonic Device. *Science* **2019**, *366*, 1121−1125.
(34) McMichael, R. D.; Stiles, M. D. Magnetic Normal Modes of Nanoelements. *J. Appl. Phys.* **2005**, *97*, 10J901.
(35) Verba, R.; Körber, L.; Schultheiss, K.; Schultheiss, H.; Tiberkevich, V.; Slavin, A. Theory of Three-Magnon Interaction in a Vortex-State Magnetic Nanodot. *Phys. Rev. B: Condens. Matter Mater. Phys.* **2021**, *103*, 014413.
(36) Grigoryeva, N. Y.; Popov, D.; Kalinikos, B. Dipole-Exchange Spin Wave Spectrum in an Anisotropic Ferromagnetic Waveguide with a Rectangular Cross Section. *Phys. Solid State* **2014**, *56*, 1806−1816.
(37) Camley, R. E. Three-Magnon Processes in Magnetic Nanoelements: Quantization and Localized Mode Effects. *Phys. Rev. B: Condens. Matter Mater. Phys.* **2014**, *89*, 214402.
(38) Barsukov, I.; Fu, Y.; Safranski, C.; Chen, Y.-J.; Youngblood, B.; Gonçalves, A. M.; Spasova, M.; Farle, M.; Katine, J. A.; Kuo, C. C.; Krivorotov, I. N. Magnetic Phase Transitions in Ta/CoFeB/MgO Multilayers. *Appl. Phys. Lett.* **2015**, *106*, 192407.
(39) Parkin, S. S. P. Systematic Variation of the Strength and Oscillation Period of Indirect Magnetic Exchange Coupling Through the 3d, 4d, and 5d Transition Metals. *Phys. Rev. Lett.* **1991**, *67*, 3598−3601.
(40) Gonçalves, A. M.; Garcia, F.; Lee, H. K.; Smith, A.; Soledade, P. R.; Passos, C. A. C.; Costa, M.; Souza-Neto, N. M.; Krivorotov, I. N.; Sampaio, L. C.; Barsukov, I. Oscillatory Interlayer Coupling in Spin Hall Systems. *Sci. Rep.* **2018**, *8*, 1−6.
(41) Barsukov, I.; Fu, Y.; Gonçalves, A. M.; Spasova, M.; Farle, M.; Sampaio, L. C.; Arias, R. E.; Krivorotov, I. N. Field-dependent Perpendicular Magnetic Anisotropy in CoFeB Thin Films. *Appl. Phys. Lett.* **2014**, *105*, 152403.
(42) Yuasa, S.; Nagahama, T.; Fukushima, A.; Suzuki, Y.; Ando, K. Giant Room-Temperature Magnetoresistance in Single-Crystal Fe/MgO/Fe Magnetic Tunnel Junctions. *Nat. Mater.* **2004**, *3*, 868−871.
(43) Gonçalves, A. M.; Barsukov, I.; Chen, Y. J.; Yang, L.; Katine, J. A.; Krivorotov, I. N. Spin Torque Ferromagnetic Resonance With Magnetic Field Modulation. *Appl. Phys. Lett.* **2013**, *103*, 172406.
(44) Ishibashi, M.; Shiota, Y.; Li, T.; Funada, S.; Moriyama, T.; Ono, T. Switchable Giant Nonreciprocal Frequency Shift of Propagating Spin Waves in Synthetic Antiferromagnets. *Sci. Adv.* **2020**, *6*, eaaz6931.
(45) Jenkins, S.; Meo, A.; Elliott, L. E.; Piotrowski, S. K.; Bapna, M.; Chantrell, R. W.; Majetich, S. A.; Evans, R. F. L. Magnetic Stray Fields in Nanoscale Magnetic Tunnel Junctions. *J. Phys. D: Appl. Phys.* **2020**, *53*, 044001.
(46) Tyberkevych, V.; Slavin, A.; Artemchuk, P.; Rowlands, G. Vector Hamiltonian Formalism For Spin-wave Dynamics. *arXiv:2011.13562*, 2020.
(47) Dieterle, G.; Förster, J.; Stoll, H.; Semisalova, A. S.; Finizio, S.; Gangwar, A.; Weigand, M.; Noske, M.; Fähnle, M.; Bykova, I.; Gräfe, J.; Bozhko, D. A.; Musiienko-Shmarova, H. Yu.; Tiberkevich, V.; Slavin, A. N.; Back, C. H.; Raabe, J.; Schütz, G.; Wintz, S. Coherent Excitation of Heterosymmetric Spin Waves with Ultrashort Wavelengths. *Phys. Rev. Lett.* **2019**, *122*, 117202.
(48) Verba, R. V.; Hierro-Rodriguez, A.; Navas, D.; Ding, J.; Liu, X. M.; Adeyeye, A. O.; Guslienko, K. Y.; Kakazei, G. N. Spin-wave Excitation Modes in Thick Vortex-State Circular Ferromagnetic Nanodots. *Phys. Rev. B: Condens. Matter Mater. Phys.* **2016**, *93*, 214437.
(49) Vansteenkiste, A.; Leliaert, J.; Dvornik, M.; Helsen, M.; Garcia-Sanchez, F.; van Waeyenberge, B. The Design and Verification of MuMax3. *AIP Adv.* **2014**, *4*, 107133.
(50) Sun, J.; Ralph, D. Magnetoresistance and Spin-Transfer Torque in Magnetic Tunnel Junctions. *J. Magn. Magn. Mater.* **2008**, *320*, 1227−1237.

(51) Spicer, T. M.; Keatley, P. S.; Loughran, T. H. J.; Dvornik, M.; Awad, A. A.; Dürrenfeld, P.; Houshang, A.; Ranjbar, M.; Åkerman, J.; Kruglyak, V. V.; Hicken, R. J. Spatial Mapping of Torques Within a Spin Hall Nano-Oscillator. *Phys. Rev. B: Condens. Matter Mater. Phys.* **2018**, *98*, 214438.
(52) Wang, C.; Cui, Y.-T.; Sun, J. Z.; Katine, J. A.; Buhrman, R. A.; Ralph, D. C. Bias and Angular Dependence of Spin-Transfer Torque in Magnetic Tunnel Junctions. *Phys. Rev. B: Condens. Matter Mater. Phys.* **2009**, *79*, 224416.
(53) Chumak, A. V.; Vasyuchka, V. I.; Serga, A. A.; Hillebrands, B. Magnon Spintronics. *Nat. Phys.* **2015**, *11*, 453−461.

https://doi.org/10.1021/acsami.1c01562
ACS Appl. Mater. Interfaces 2021, 13, 20288−20295